Available online at www.sciencedirect.com
ScienceDirect
Remote Sensing of Environment 112 (2008) 456–470
Remote Sensing of Environment
www.elsevier.com/locate/rse

Quantifying the impact of cloud obscuration on remote sensing of active fires in the Brazilian Amazon

Wilfrid Schroeder [a,*], Ivan Csiszar [a], Jeffrey Morisette [b]

[a] Department of Geography, University of Maryland, College Park, MD 20742, United States
[b] NASA's Goddard Space Flight Center Code 614.5 Greenbelt, MD 20771, United States

Received 19 December 2006; received in revised form 12 April 2007; accepted 6 May 2007

Abstract

Vegetation fires remain as one of the most important processes governing land use and land cover change in tropical areas. The large area extent of fire prone areas associated with human activities makes satellite remote sensing of active fires a valuable tool to help monitor biomass burning in those regions. However, identification of active fire fronts under optically thick clouds is not possible through passive remote sensing, often resulting in omission errors. Previous analyses of fire activity either ignored the cloud obscuration problem or applied corrections based on the assumption that fire occurrence is not impacted by the presence of clouds. In this study we addressed the cloud obscuration problem in the Brazilian Amazon region using a pixel based probabilistic approach, using information on previous fire occurrence, precipitation and land use. We implemented the methodology using data from the geostationary GOES imager, covering the entire diurnal cycle of fire activity and cloud occurrence. Our assessment of the method indicated that the cloud adjustment reproduced the number of potential fires missed within 1.5% and 5% of the true fire counts on annual and monthly bases respectively. Spatially explicit comparison with high resolution burn scar maps in Acre state showed a reduction of omission error (from 58.3% to 43.7%) and only slight increase of commission error (from 6.4% to 8.8%) compared to uncorrected fire counts. A basin-wide analysis of corrected GOES fire counts during 2005 showed a mean cloud adjustment factor of approximately 11%, ranging from negligible adjustment in the central and western part of the Brazilian Amazon to as high as 50% in parts of Roraima, Para and Mato Grosso.

Keywords: Vegetation fires; Clouds; Geostationary satelite; Brazilian amazon

1. Introduction

Vegetation fires play a significant role in land and atmospheric processes globally. Their occurrence is particularly important in tropical regions where human activity is still heavily based on the use of fires for land use management and land cover change. In the latter case, deforestation and fires are found to be closely related eventually leading to important feedback processes that favor faster and more destructive depletion of the local forests (Cochrane et al., 1999; Nepstad et al., 1999). In contrast, at higher latitude regions a greater percentage of fires are caused by lightning or are accidental in nature and are highly influenced by the local weather and climate conditions (Kasischke et al., 2002). Fires in the tropics are influenced by local conditions too but will also present an equally important component due to the influence of human activities which are reflected in the spatial and temporal distributions observed across regional to global scales (Barbosa et al., 1999; Scholes et al., 1996).

Correct quantification of fire events is needed primarily for understanding the dynamics of land use and land cover change and therefore subsidize regional environmental programs, as well as for providing information for modeling of emission estimates from biomass combustion (Korontzi et al., 2004; Van der Werf et al., 2003). Consideration of the fire diurnal cycle is also required for biomass burning transport models, making high observation frequency a particularly important characteristic on active fire monitoring systems (Freitas et al., 2005; Giglio et al., 2006). Satellite sensors have been used to monitor vegetation fire activity for many years now, providing greater

* Corresponding author. 2181 LeFrak Hall, Department of Geography, University of Maryland, College Park, MD 20742, United States.
E-mail address: schroeder@hermes.geog.umd.edu (W. Schroeder).

0034-4257/$ - see front matter © 2007 Elsevier Inc. All rights reserved.
doi:10.1016/j.rse.2007.05.004

insight on the processes associated with fire dynamics at different scales (Bucini & Lambin, 2002; Carmona-Moreno et al., 2005; Di Bella et al., 2006; Dwyer et al., 2000; Giglio et al., 2006). In fact, the use of satellite data is the only way to assess fire activity at spatial and temporal scales required for land surface and atmospheric modeling studies. However, the remote sensing methods used for monitoring fires have limitations that tend to cause important biases in the final products (Boles & Verbyla, 2000; Cardoso et al., 2005; Eva & Lambin, 1998; Kasischke et al., 2003; Schroeder et al., 2005). A major factor influencing fire numbers derived from remotely sensed data is the effect caused by cloud obscuration. Because fires have their highest spectral emission values located in the mid-infrared band, active fire products exploit that part of the spectrum to distinguish biomass burning events from the surrounding background (Giglio et al., 1999; Justice et al., 2002). The presence of optically thick clouds along the atmospheric path between the target (fire) and the satellite sensor will, however, greatly reduce the ability to detect a fire due to severe attenuation of the spectral signal emitted by either flaming or smoldering phases of biomass combustion. The extent of the effect of cloud obscuration on fire detection will depend on the average cloud cover fraction. But it should be realized that clouds are needed to produce rain but are not necessarily followed by precipitation. Also the extent and degree of human activities will influence the spatial and temporal fire distributions.

Current methods used to compensate satellite active fire detection to account for fires missed due to cloud obscuration tend to rely on the assumption that fires occur with the same frequency under cloud covered areas as they do in the open (Cardoso et al., 2003; Giglio et al., 2003, 2006; Roberts et al., 2005). Despite being an attractive approach for its simplistic assumption, the adoption of such procedures becomes problematic in areas where fires are unevenly distributed in space. Under such conditions, the resulting adjustment numbers will be potentially influenced by the cell size selected to extrapolate the applicable clear sky fire density to the complementary cloud covered area. The major implication of such an approach is associated with the assumption of fires in areas with no burning activity which would lead to an overestimation of fire numbers. Here we present an approach that uses precipitation data and land use information to more precisely quantify the potential omission error associated with the cloud obscuration affecting satellite active fire detection products. The proposed approach is applied to a geostationary satellite fire data set, in order to characterize the cloud effect on fire detection over the entire diurnal cycle. The analyses are focused on the Brazilian Amazon where intense fire activity and frequent cloud cover are prevalent (Fig. 1). In the sections to follow we describe the data sets used and the method developed and present the results produced for 2005.

2. Data

2.1. Active fire product

In the past two decades multiple satellite-based active fire products have been designed using a variety of sensors (Elvidge et al., 1996; Giglio et al., 2000; Kaufman et al., 1990, 1998a; Menzel et al., 1991). The performance of individual products is found to be strongly dependent on the sensor's spectral characteristics and on the algorithm used, as well as on the imaging characteristics (e.g., pixel size, observation geometry) provided by the instruments and the orbital platforms on which

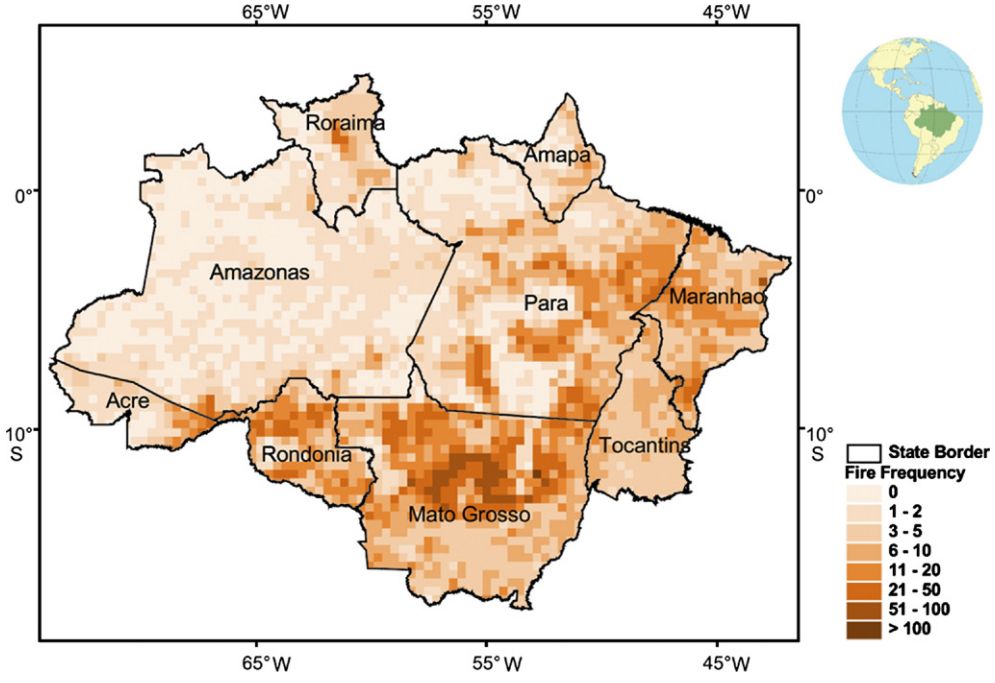

Fig. 1. Fire frequency (fires 10^{-2} km^{-2} year^{-1}) across the nine Brazilian States in Amazonia. Values based on 3-year average (2003–2005) GOES WFABBA fire detection data using all observation hours available.

they are mounted (Morisette et al., 2005; Schroeder et al., 2005). Despite their usual coarser spatial resolution, geostationary satellites are extremely interesting for fire monitoring as they provide high observation frequency. High frequency observations are important for deriving the diurnal cycle of fire activity at the regional to basin-wide level as well as for modeling time dependent transport of biomass burning emissions (Freitas et al., 2005).

Data from the Geostationary Operational Environmental Satellite positioned at 75° longitude (GOES-East) are used in this study. The GOES-East satellite is located over the study area selected, the Brazilian Amazon, thereby offering near optimal observation conditions (i.e., near nadir viewing geometry) for fire detection. The nominal 4×4 km pixel resolution at subsatellite position remains stable throughout most of the region with less than 25% increase in pixel area being observed near the far most corners of the study area.

Two major GOES-based operational active fire products are available for the study area. The Wildfire Automated Biomass Burning Algorithm (WFABBA) is produced by the University of Wisconsin — Madison and uses a contextual approach for detecting active fires (Prins & Menzel, 1992; Prins et al., 1998). This product is available for the period of 2000–present and covers the entire study area. The other product is generated by the Weather Forecast and Climate Studies Center in Brazil (CPTEC) and combines fixed threshold and contextual tests for detecting fires (CPTEC/INPE, 2005); data are available from July 2004 to present. Because of limited temporal coverage found with the latter, we used WFABBA's active fire product in this study. The data set selected for use covers the period of January 2003–December 2005 and is composed of 17,520 half hourly files per year. Each file contains information on fire location and acquisition date along with the temperature and area estimates and the assigned confidence for each detection. The latter is divided into five categories ranging from high (0) to low (5) confidence. Category 5 was rejected here as in some cases it was found to be strongly associated with spurious detections composed of large clusters of pixels with no similar detections from other sensors. This observation confirmed the expectations for the performance of this particular product in relation to commission errors (Elaine Prins — personal communication, 2005). Previous validation of WFABBA's fire product performed during the Smoke, Clouds and Radiation-Brazil (SCAR-B) experiment, showed that forest conversion fires as small as 1 ha could be detected by that algorithm (Prins et al., 1998). WFABBA's active fire detection product was selected as the source data to which the cloud obscuration adjustments were implemented based on the methodology described in Section 3. The necessary WFABBA product files were made available by the University of Wisconsin — Madison.

2.2. Precipitation data

The second set of data used in this study was the satellite derived precipitation estimates. The Brazilian Amazon is still only partially covered by meteorological and hydrological surface stations from which precipitation data can be extracted. Rainfall is generated primarily within localized convective systems leading to potential effects on the quality of the precipitation estimates based on spatially interpolated surface station data from the region (Costa & Foley, 1998). Availability of meteorological radar data is also scarce due to limited spatial and temporal coverage. Consequently, the use of radar data was not considered as a viable alternative for this study. Because of these limitations, satellite derived precipitation products were used for assessing rainfall conditions throughout the Brazilian Amazon. As with the remote sensing of active fires, precipitation estimates are provided by different sensors using different algorithms that can be based on single instrument or on multi-sensor multi-data approaches (Bellerby et al., 2001; Kummerow et al., 1998; Rudolf et al., 1996). Consideration of the spatial and temporal resolutions and the accuracy of the precipitation products that have achieved operational mode led to the use of GOES-based precipitation estimates for this study. CPTEC currently generates daily GOES-based precipitation estimates for most of South America at the nominal spatial resolution of 4×4 km. CPTEC's product is a revised version of the Hydro-estimator method (Vicente et al., 1998) which uses improved coefficients for the specific conditions observed over Brazil (Vila & Lima, 2004; Carlos Frederico Angelis — personal communication, 2005). CPTEC's GOES-based precipitation estimates data production was initiated in January 2004 providing daily files with total accumulated precipitation at nominal 4 km resolution. The data set used in this study covers January 2004–December 2005.

Prior to the application of CPTEC's Hydro-estimator precipitation data to the proposed methodology, an evaluation was performed using point precipitation data obtained from 19 automated surface weather stations available across the basin (URL: http://tempo.cptec.inpe.br:9080/PCD/). Fig. 2A–C show the results for all stations selected using three different time integration periods — 1, 7, and 30 days, respectively. The correlation between the two data sets is seen to improve significantly with the total number of days used in the sampling process.

Two major factors were believed to contribute to the dispersion seen in all three graphs. First, there is the natural difficulty in relating the surface station's point data to the 4×4 km pixel footprint as obtained with the GOES data. The large rainfall spatial heterogeneity mentioned above will cause significant impact on the area averaged estimates produced from the satellite data. The effect of the spatial variability in precipitation patterns in the region is exemplified in Fig. 2D, where the absolute difference calculated for the satellite and surface station precipitation values is plotted against the satellite precipitation variance (σ^2) based on 9 pixels centered at one surface station location.

Another important factor contributing to the dispersion seen in Fig. 2A–C is related to the inherent deficiencies in the precipitation product that are associated with the use of passive remote sensing data from GOES and empirical relationships that tend to impact the accuracy of the precipitation estimates produced (Boi et al., 2004; Ebert et al., 2007; Rozumalski, 2000; Vicente et al., 2002). Despite these limitations, the high observation frequency of the GOES precipitation estimates

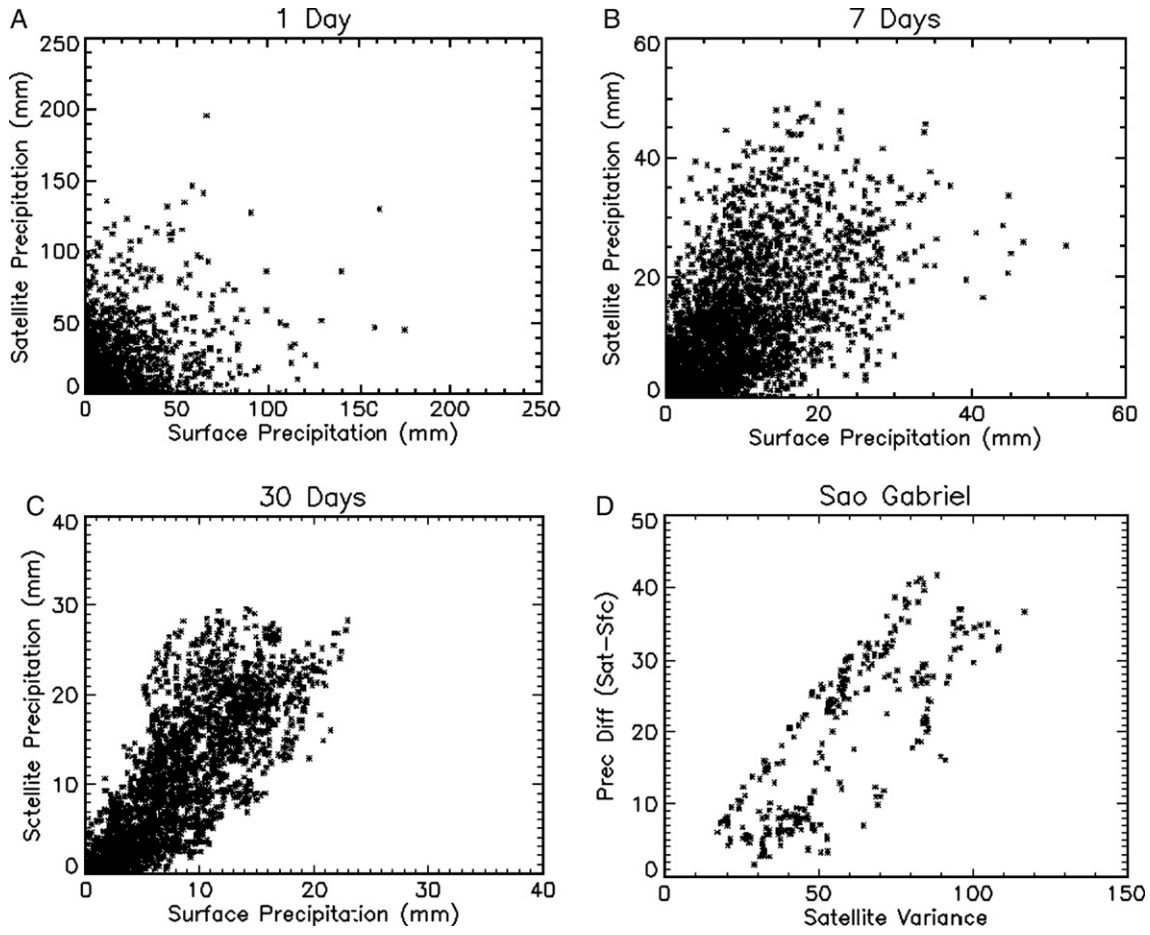

Fig. 2. Scatter plots of the satellite precipitation estimates and the surface precipitation observations using 1(A), 7(B) and 30 (C) day average values and of the difference between the satellite precipitation estimates and the surface precipitation data and the satellite variance (D) calculated for the 9 pixels centered at the Sao Gabriel weather station in Amazonas state.

allows for improved integration of the 24 h precipitation totals thereby providing valuable information for use in this study. Also, as will be described in Section 3.1, our approach will be based on relative differences between precipitation estimates making absolute accuracy of the product of less significance.

2.3. Cloud mask

The WF-ABBA fire product consists of a list of fire detections, but no cloud mask is included. However, a cloud mask is needed for identifying cloud obscured pixels that require processing for potential fire omission. Therefore we developed a new cloud product at the 4 km spatial and 30 min temporal resolution of the original active fire data, which is the basis of the cloud obscuration processing scheme. The cloud mask was designed based on the use of the Global-Merged Infra-Red Brightness Temperature (from here on designated simply as BT) product generated by the Climate Prediction Center (CPC, 2005). The BT data are a single band global product derived from multiple geostationary satellite imagery and gridded to nominal 4 × 4 km resolution. In the case of the Brazilian Amazon the BT product is primarily derived from GOES-East imagery. Specific criteria based on the regional conditions were applied to derive the cloud mask product used in this study. The unique conditions of the Amazon region in terms of daily BT trends were explored to derive a method that uses fixed and dynamic thresholds to distinguish between clouds and land surfaces in the BT images. Daily variation of BT is small for clear sky pixels as surface temperature remains much constant within a 30 day period (Alvalá et al., 2002). The stability of surface conditions is demonstrated in Fig. 3B in which a typical pattern of BT values extracted from a 30 day profile obtained from the same pixel and observation hour is presented. The set of empirically defined tests used in the production of the cloud masks is summarized bellow:

$$BT_i \leq 237\ K \rightarrow \text{ Super Cold Cloud} \quad \text{(i)}$$

$$BT_i > 237\ K \text{ and } BT_i \leq 278\ K \rightarrow \text{Cold Cloud} \quad \text{(ii)}$$

$$BT_i > 278\ K \text{ and } BT_i < \overline{BT_{n=30}} - 1.5 \times \sigma_{n=30} \rightarrow \text{Warm/Subpixel Cloud} \quad \text{(iii)}$$

$$BT_i > 278\ K \text{ and } BT_i \geq \overline{BT_{n=30}} - 1.5 \times \sigma_{n=30} \rightarrow \text{Clear Sky.} \quad \text{(iv)}$$

Where BT is evaluated for each individual pixel imaged during the *i*th observation hour. Conditions (iii–iv) use information from the previous 30 days for calculating the mean ($\overline{\mathrm{BT}}$) and the standard deviation (σ) for observation hour *i*. Only pixels having *BT* values greater than 278 K are considered in the calculation of $\overline{BT}$ and σ. The cloud mask processing also requires that a minimum of 10% of the BT data available during the 30 day sampling period be greater than 278 K. The threshold of 278 K was found to work well for this specific data set as it provided the dividing line between unambiguous cloudy pixels and other surfaces. Having a minimum of 10% of all values observed within a 30 day period above 278 K was then required to estimate the approximate clear sky BT value and therefore allows for proper classification of the pixels. For those cases where this criterion is not met, the pixels are classified as *undetermined* and thereby not used in the cloud obscuration processing. Approximately 1.5% of the pixels analyzed were classified as undetermined.

The performance of the cloud mask product was tested against another source (CPTEC's GOES-based operational multi-band daytime-only cloud classification method; http://satelite.cptec.inpe.br) to check for consistency. Two 20 day periods were analyzed: one in the wet season (February 2005) and one in the dry season (September 2005). The results showed the two products to be in good agreement and proved the cloud mask to be effective in identifying cloudy pixels (>95% correspondence with CPTEC's classification during both wet and dry seasons). Pixels classified as cloud-free by the cloud mask product showed a less significant agreement with CPTEC's product (23% during the wet season and 56% during the dry season). To help explain the differences between the two products we randomly selected approximately 20 cases from the wet and dry seasons for which GOES 1 km and MODIS 1 km and 500 m bands were visually inspected. The visual analysis suggested that sub-pixel cumulus clouds that are routinely observed in the Amazon basin as well as other sorts of contaminants (e.g., thin cirrus clouds, smoke plumes) are more frequently classified as *clouds* by the more conservative method used by CPTEC resulting in the differences found.

Half hourly global BT files were obtained from the NASA's Goddard Space Flight Center Distributed Active Archive Center (DAAC) covering years 2004 and 2005 (17,520 files per year) and the cloud mask algorithm was applied for the Brazilian Amazon spatial subset. Analysis of the BT data showed that pixels having confirmed measurable precipitation (based on precipitation observations derived from the same surface station network used to evaluate the hydro-estimator product above) had a mean value of 237 K (σ=22 K). This result corroborates the findings of Arkin (1979) who obtained a 0.75 correlation coefficient between surface precipitation data and three month-average satellite rainfall estimates for brightness temperature values lower than 235 K. Based on this finding, the cloud obscuration analysis was only carried for pixels showing BT values greater than 237 K during the 24 h period between the last satellite precipitation estimate available and the following one.

3. Methods

In order to predict whether there are fires present under clouds, we need to determine the conditions under which fires are likely to occur. In the case of the Brazilian Amazon region, both physical and social factors play important roles in defining where and when fires occur. The methodology presented here uses precipitation estimates to determine the physical conditions of the environment, along with previous active fire data to derive the spatial and temporal distributions of fires that are known to be influenced by specific land use patterns observed throughout the region. Given that the extent of the Brazilian Amazon is over 5 million km^2, the conditions leading to vegetation fires can vary significantly across the region. The existence of vegetation cover types ranging from grasslands to closed canopy evergreen forests requires that the area be divided into smaller parts in order to represent local characteristics of fire occurrence. Consequently a 40×40 km grid covering the study area (3358 cells total) was used to stratify the entire basin into smaller subparts. The grid size selected was meant to preserve the small scale phenomena represented in the analyses while balancing the need for reasonable sample sizes required to produce the summary statistics described below. In addition, the selected grid size allowed for easier association with the nominal 4×4 km GOES pixel distribution. Analyses of the physical conditions and spatial and temporal dynamics was undertaken for each one of the 48 daily GOES observation hours (30 min interval). In the following sections we describe the relationships used to determine potential fire omissions due to cloud.

3.1. Fire dynamics and precipitation

Precipitation will have a great impact on the conditions of the local environment, influencing the mechanisms that control vegetation moisture content and temperature and the latent and sensible heat fluxes that affect land surface and atmospheric humidity and temperature conditions (Betts et al., 2002; Bruno et al., 2006; Nepstad et al., 2002). WFABBA active fire data from 2004–2005 were used in conjunction with the GOES precipitation estimates for the same period to derive the physical conditions that facilitate fire development. Precipitation amounts during the 30 day period preceding each fire detection were extracted for every observation hour and the information gridded to the 40×40 km grid:

$$RT_{i,n,z} = \left[\sum_{\mathrm{day}=-1}^{\mathrm{day}=-1} r_n, \sum_{\mathrm{day}=-1}^{\mathrm{day}=-2} r_n, \ldots, \sum_{\mathrm{day}=-1}^{\mathrm{day}=-30} r_n \right]. \quad (1)$$

Where *RT* is a 30 element array containing the accumulated precipitation *r* during a 30 day period preceding fire *n*

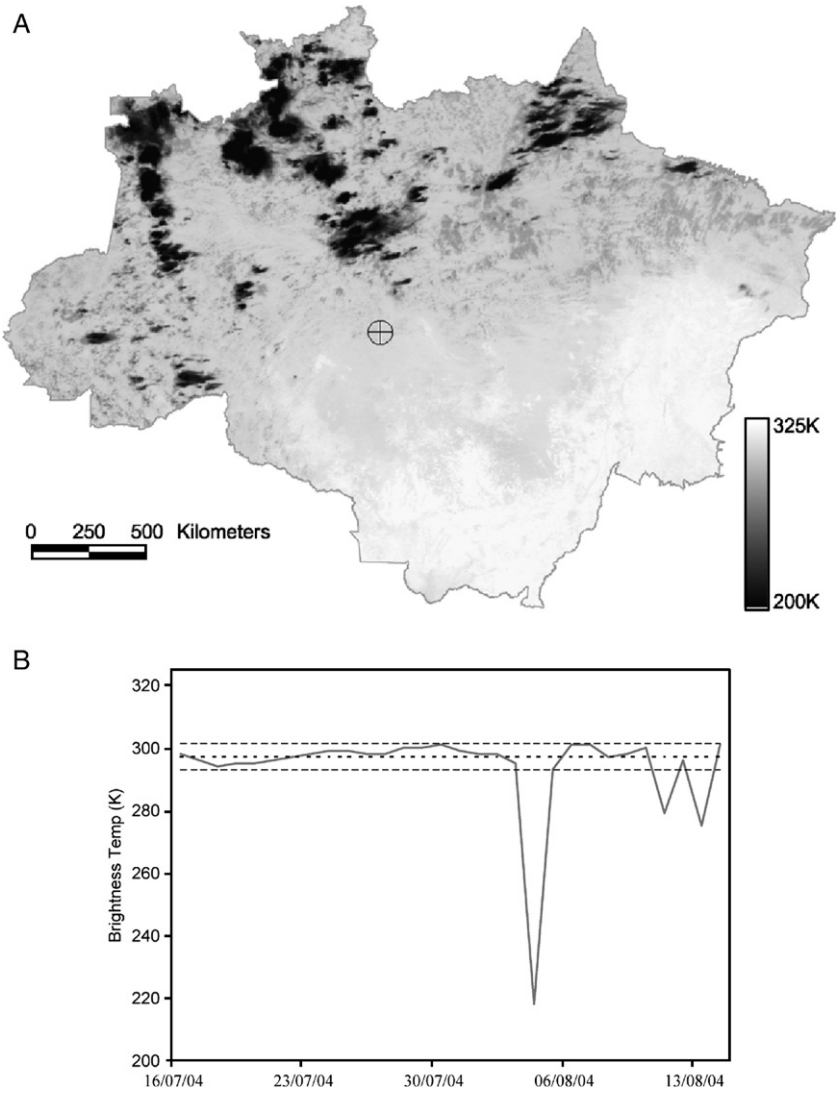

Fig. 3. Brightness temperature (BT) image for 15 August 2004 1815 h UTC (A) and the 30 day (July 16 → August 15 2004) temporal profile (B) for the pixel marked as "⊕" on the image. Solid line represents the observed BT values, the dotted line represents the 30 day mean value, and the dashed lines the 30 day standard deviation.

[$n=1,\ldots, N$] detected during observation hour i [$i=1,\ldots, 48$] and located in grid cell z [$z=1,\ldots, 3358$]. A third degree polynomial was adjusted to the mean values representing the group of data found in each one of the 40×40 km grid cells for each observation hour.

$$\overline{Ri}, z = \left(\frac{\sum_{n=1}^{n=N} RT_{i,n,z}[1]}{N}, \frac{\sum_{n=1}^{n=N} \mathrm{RT_{i,n,z}}[2]}{\mathrm{N}}, \ldots, \frac{\sum_{n=1}^{n=N} \mathrm{RT_{i,n,z}}[30]}{\mathrm{N}} \right) \quad (2)$$

$$M_{i,z} = \left\{ (1, \overline{Ri}, z[1]), (2, \overline{Ri}, z[2]), \ldots, (30, \overline{Ri}, z[30]) \right\}. \quad (3)$$

$$f_{i,z}(x) = a_0 + a_1 x + a_2 x^2 + a_3 x^3. \quad (4)$$

Where $\overline{R}$ is the 30 element array with the mean accumulated precipitation for N fires detected during observation hour i at cell z, and M is the resulting array of data for which the coefficients in Eq. (4) are calculated for. Eq. (4) is the function defining the relationship between the number of days (x) preceding a fire and the respective mean accumulated precipitation for that period. Interestingly, M assumes a strong linear distribution when N grows larger (typically for $N>50$) (Fig. 4). The application of a third degree polynomial proved a good fit with most conditions observed. The resulting curve coefficients were stored in individual look up tables (LUT, one for each observation hour) and were to be used in the final code as a reference value describing the mean precipitation conditions preceding fires at each 40×40 km grid cell.

The information provided by the polynomial curves was used to set the probability ranges that describe the potential occurrence of fires based on the physical condition of the

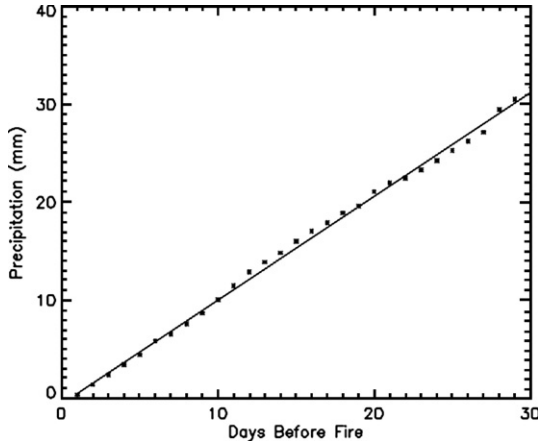

Fig. 4. Mean precipitation values calculated for a single 40×40 km cell (approx. location: 60.10 °W 12.50 °S) based on N=151 active fire detections observed during 2004–2005. R^2=0.9974.

environment as defined by the precipitation data. The criteria used to determine the probability of fire occurrence as a function of precipitation were the following:

$$\sum_{\text{day}=1}^{\text{day}=30} RA_{i,z} \leq \int_1^{30} f_{i,z}(x)\mathrm{d}x \rightarrow P_R = 1 \tag{5}$$

$$\left\{ \begin{array}{c} \sum_{\text{day}=1}^{\text{day}=30} RA_{i,z} > \int_1^{30} f_{i,z}(x)\mathrm{d}x \\ \text{and} \\ \sum_{\text{day}=1}^{\text{day}=30} RA_{i,z} \leq 2\int_1^{30} f_{i,z}(x)\mathrm{d}x \end{array} \right\} \rightarrow P_R = \int_1^{30} (x)\mathrm{d}x - \frac{\sum_{\text{day}=1}^{\text{day}=30} RA_{i,z}}{\int_1^{30} f_{i,z}(x)\mathrm{d}x}. \tag{6}$$

Where RA is the actual precipitation data that is accumulated over the 30 day period for a particular pixel at observation hour i and grid cell z, $\int \mathrm{d}x$ is time integral (30 days) calculated for the polynomial curve $f(x)$, and P_R is the assigned probability of fire occurrence related to precipitation. According to Eqs. (5) and (6), RA must be less than two times the area defined by the LUT curve covering the 30 day period for a particular location and observation hour for the pixel to be considered for the cloud obscuration analysis. Additionally, a third test was implemented to avoid particular conditions when the actual precipitation is concentrated in the most recent period (day-1 → day-7). This test is based on anecdotal evidence, which suggests that land owners in the region normally wait for approximately one week to burn following a rainfall episode. In this case, a more conservative approach is applied using the criteria:

$$\sum_{\text{day}=1}^{\text{day}=7} RA_{i,z} \geq \int_1^{30} f_{i,z}(x)\mathrm{d}x \rightarrow P_R = 0. \tag{7}$$

From the above test, for the pixel to be considered for the cloud obscuration processing, the actual precipitation recorded during the 7 day period preceding an observation cannot be greater than the 30 day mean precipitation associated with fires for that same location and observation hour.

3.2. Fire spatial and temporal dynamics

Fire activity in tropical areas tends to follow very specific patterns as a function of land use and land cover change. In those areas, the systematic use of fires for land clearing and maintenance creates reasonably consistent spatial and temporal patterns in satellite active fire detection from year to year (Giglio et al., 2006). To establish the mean annual fire activity in time and space over the Brazilian Amazon, we used active fire records derived from GOES during 2003–2004. The 40×40 km grid used to extract the fire and precipitation relationship was also applied in this analysis.

In order to derive the temporal distribution of fires, the year was divided into 26 14-day periods. We used 14 day period intervals to properly represent the seasonal curves of fire activity. Fire seasons were usually constrained to approximately 2–3 months, thereby 14 day periods allowed for a good representation of the progress in fire activity throughout the season while keeping our samples for each cell to a reasonable size. The probability distribution of fires detected during each one of the 14-day periods in relation to the 2003–2004 totals was calculated for all 40×40 km grid cells according to:

$$P_{Tz}(t) = \frac{\sum_{t}^{2004} \text{fires}_z}{\sum_{2003}^{2004} \text{fires}_z}. \tag{8}$$

Where P_T is the active fire probability distribution for grid cell z, the numerator represents the number of fires detected during a 14 day period t, and the denominator represents the total number of fires observed in grid cell z during the entire period analyzed (2003–2004). An LUT containing the results for each grid cell was produced for every observation hour to be used in the final code. To reduce the effects of the inter-annual variability in fire activity on the adjustment factors produced, we used information from the year for which the processing was implemented (in this case 2005) to account for departs from the mean values described by the LUTs containing the P_T data described above. For this we used a metrics P_{14} describing the

Table 1
Fire return rate based on GOES WFABBA active fire product using a 4×4 km grid covering the Brazilian Amazon

Years with detection	1745UTC	All hours included
2003 and 2004	33%	68%
2004 and 2005	40%	65%
2003 and 2005	33%	66%
2003 and 2004 and 2005	19%	52%

Values represent the percentage of all cells with fire activity in one year that also showed detections in subsequent years based on (i) the observation hour of 1745UTC and (ii) all observation hours.

sum of fires detected during the preceding 14 day period for each 40 km grid cell that was systematically updated during processing. Therefore, any increase or decrease in fire activity for a particular grid cell would be considered in the calculation of the cloud obscuration adjustment produced by either increasing or decreasing the contribution from the term P_T in Eq. (8) relatively to P_{14}.

In addition to the annual distribution of fires observed with the active fire data record from 2003–2004, evaluation of fire's return frequency was also conducted. Vegetation fires are usually associated with a high return frequency in tropical regions (Cochrane & Schulze, 1999). The analysis of GOES active fire data during the period of 2003–2005 including all observation hours showed that approximately 66% of the areas under the influence of fires in one year also exhibited some activity in the following year (Table 1). However, the likelihood of observing a fire in a particular area during the same observation hour over sequential years becomes much less evident. Multiple factors were believed to contribute to the latter, including but not limited to changes in the hour of the day a fire is ignited, changes in the fuel load affecting fire intensity and duration therefore impacting detectability, changes in land use, etc. Modeling these factors and the interactions among them is difficult and was not attempted here. In order to account for this greater variability when analyzing observation hours individually a random function (ξ) was used with the cloud obscuration analysis to represent fire return probability at every hour. This random function was adjusted to uniformly represent the average ranges of return probabilities at the individual observation hour column from Table 1.

Complementing the analysis of the land use influence in the establishment of fire patterns across the study area, the spatial distribution of fires was determined with the implementation of a 4×4 km grid nested in the previous 40×40 km grid. This finer grid was created to represent the GOES pixel map at nominal resolution. It was intended to distinguish between areas under the influence of fires where the cloud obscuration evaluation would be performed from areas with no fire activity recorded in the most recent years where no intervention was to be conducted. All 4×4 km cells showing fire activity during years 2003 and 2004 were identified and the information stored as binary values (0 — *no fire history*; 1 — *fire prone*) in individual LUTs for every observation hour. These LUTs were updated during the actual processing to account for areas of fire expansion by adding new fire prone pixels to the existing list.

3.3. Implementation and accuracy assessment

The methodology implemented during this study was designed to use the information derived from the previous steps for compensating year 2005 GOES-East fire data for the cloud obscuration of fires. GOES data were processed sequentially for every acquisition hour during year 2005 totaling 17,520 observations. For a particular observation date and time the code would initially search for all 40×40 km grid cells that, according to the temporal LUTs, are likely to show fire activity for that particular bi-week (Fig. 5). Following this first selection, all 4×4 km areas contained by the grid cells (i.e., the nominal GOES pixels) with a history of fire activity are identified. The cloud mask product that was produced for the same year (2005) is then used to search for cloudy pixels among the previously selected ones. Two major scenarios were considered during processing, each representing distinct cloud coverage conditions.

In scenario one, a cloud covered pixel is selected for observation hour T and both adjacent detections ($T-30$ min and $T+30$ min) are also obscured by clouds. In this case, the actual precipitation data is assessed and compared against the values obtained from the LUT defining the mean precipitation curve associated with fire occurrence for that area (i.e., the 40×40 km cell). Having cleared the tests established in Eqs. (5), (6) and (7), the probability of fire omission (P_F) will be derived for that pixel using Eqs. (5), (6) and (8)and the random function (ξ),

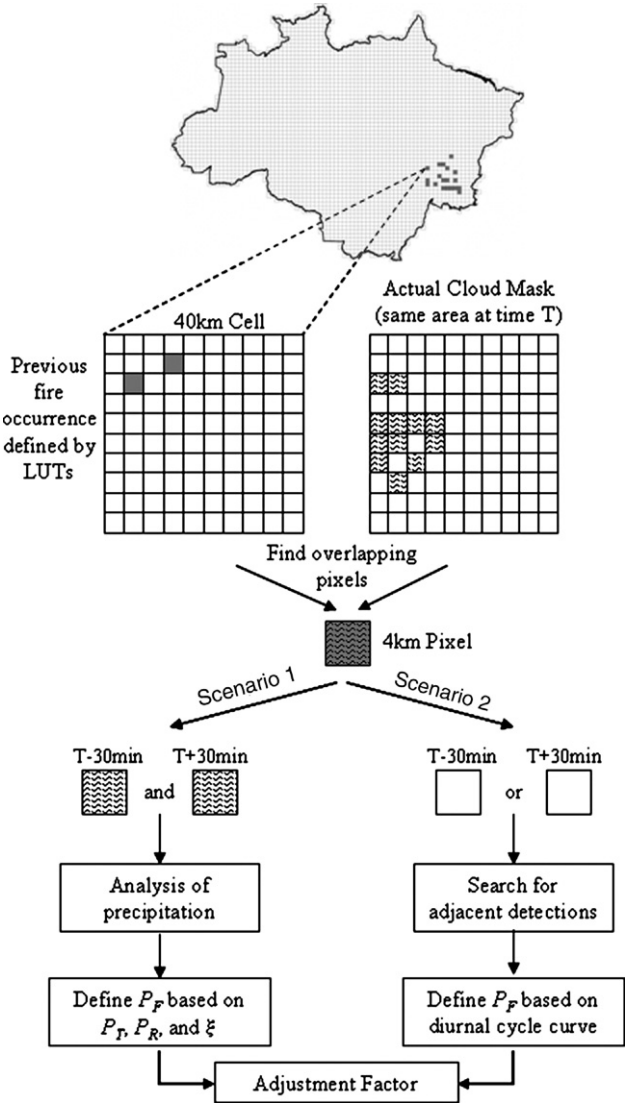

Fig. 5. Cloud obscuration processing diagram.

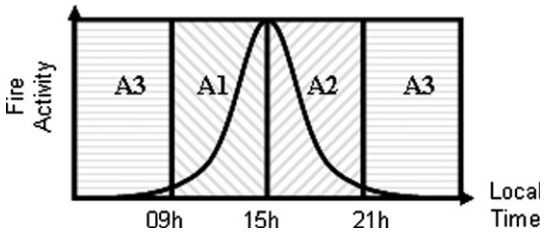

Fig. 6. Stratification of the diurnal cycle of fire activity into three major areas, A1, A2, and A3.

assuming the form:

$$P_F = P_R \times P_T \times \xi. \quad (9)$$

In scenario two, a cloudy pixel detected in time T has either the preceding ($T-30$ min) or the succeeding ($T+30$ min) observation hour cloud free. Under these conditions the code will use information from the current WFABBA fire product (searching for adjacent detections), the pixel's local time and from a general fire diurnal cycle curve. For this particular application, the curve chosen to represent the fire diurnal cycle in the region had its peak located at 1500 h local time in order to coincide with the normal hour of maximum air temperature – or inversely, minimum air humidity – (da Rocha et al., 2004) as temperature and humidity will be strongly related to fire spread conditions. The diurnal cycle curve was divided into three parts, each describing a particular trend in fire progress over time (Fig. 6). In area A1 of Fig. 6, a cloudy pixel observed at local time T_{local} will be likely to omit a fire if an actual detection exists for $T_{\text{local}}-30$ min, since fire continuation will be favored by the usual increase in temperature followed by a decrease in relative humidity. The likelihood of a fire being omitted at local time T_{local}, when detection is observed during hour $T_{\text{local}}+30$ min will depend on the potential fire occurrence during hour T_{local} for that time of the year. Based on these considerations, cloudy pixels observed during local hour T_{local} and falling within area A1 will be evaluated according to the following criteria:

Actual fire detection at $T_{\text{local}-30\ \text{min}} \rightarrow P_F = 1$ (i)

Actual fire detection at $T_{\text{local}+30\ \text{min}} \rightarrow P_F = P_T$. (ii)

In this case, if both $T_{\text{local}-30\ \text{min}}$ and $T_{\text{local}+30\ \text{min}}$ observations are cloud free, condition (i) will prevail. For area A2 in Fig. 6, a cloudy pixel observed during local hour T_{local} will have the trend in fire progress being inversely described according to the following criteria:

Actual fire detection at $T_{\text{local}-30\ \text{min}} \rightarrow P_F = P_T$ (i)

Actual fire detection at $T_{\text{local}+30\ \text{min}} \rightarrow P_F = 1$. (ii)

In this case, condition (ii) will prevail when both $T_{\text{local}-30\ \text{min}}$ and $T_{\text{local}+30\ \text{min}}$ observations are cloud free. Lastly, for area A3 in Fig. 6 a cloudy pixel detected during local hour T_{local} will receive a nominal probability P_T if either $T_{\text{local}-30\ \text{min}}$ or $T_{\text{local}+30\ \text{min}}$ observations are cloud free and a fire detection exists for any of those two observations.

To verify the consistency of the outputs produced we tested the cloud obscuration processing described above using simulated cloud coverage data in combination with the actual fire detection data from WFABBA. We used year 2005 cloud mask product to simulate the presence of clouds over randomly selected clear sky pixels found across the study area. The cloud obscuration analysis was then performed for those pixels selected in order to obtain the predicted number of fires missed due to clouds. For each pixel analyzed the actual fires detected by WFABBA were identified. The results were aggregated using the 40×40 km grid and the relationship between predicted fires versus observed fires assessed. The simulations demonstrated the predicted fires to be highly correlated with the observed fires ($R^2=0.82$) (Fig. 7). The sum of all fires produced by the cloud obscuration processing was able to represent the actual fires missed due to clouds to within 1.5% on an annual basis and to within 5% on a monthly basis.

4. Results and discussion

The main code was used to process year 2005 data and the results are presented below. The numbers produced represent those cases where a cloud obscured pixel was identified and at least one of the criteria established above was met for any of the 17,520 annual GOES observations over an area of 5.4 million km^2 (335,800 pixels at 4×4 km spatial resolution) covering the Brazilian Amazon. The probability of fire omission derived for each pixel was accumulated over multiple hours and days of observation resulting in a total number of fires potentially missed due to the presence of clouds equivalent to 59,650, or approximately 11% of the actual GOES fires detected during 2005 (545,286 total — representing WFABBA's fire types 0–4 only; category 5 associated with low probability fires not considered) (Fig. 8). The 2005 data set was also processed using the simple approach for compensating for clouds, which is based on the assumption that fires occur at the same frequency under

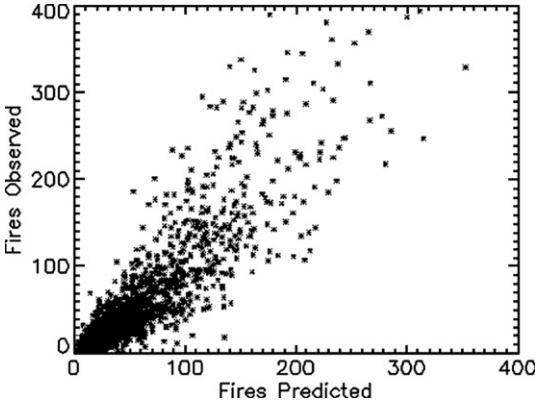

Fig. 7. Relationship between fires produced by the cloud obscuration processing based on simulated data and observed fires for the same locations using 2005 data.

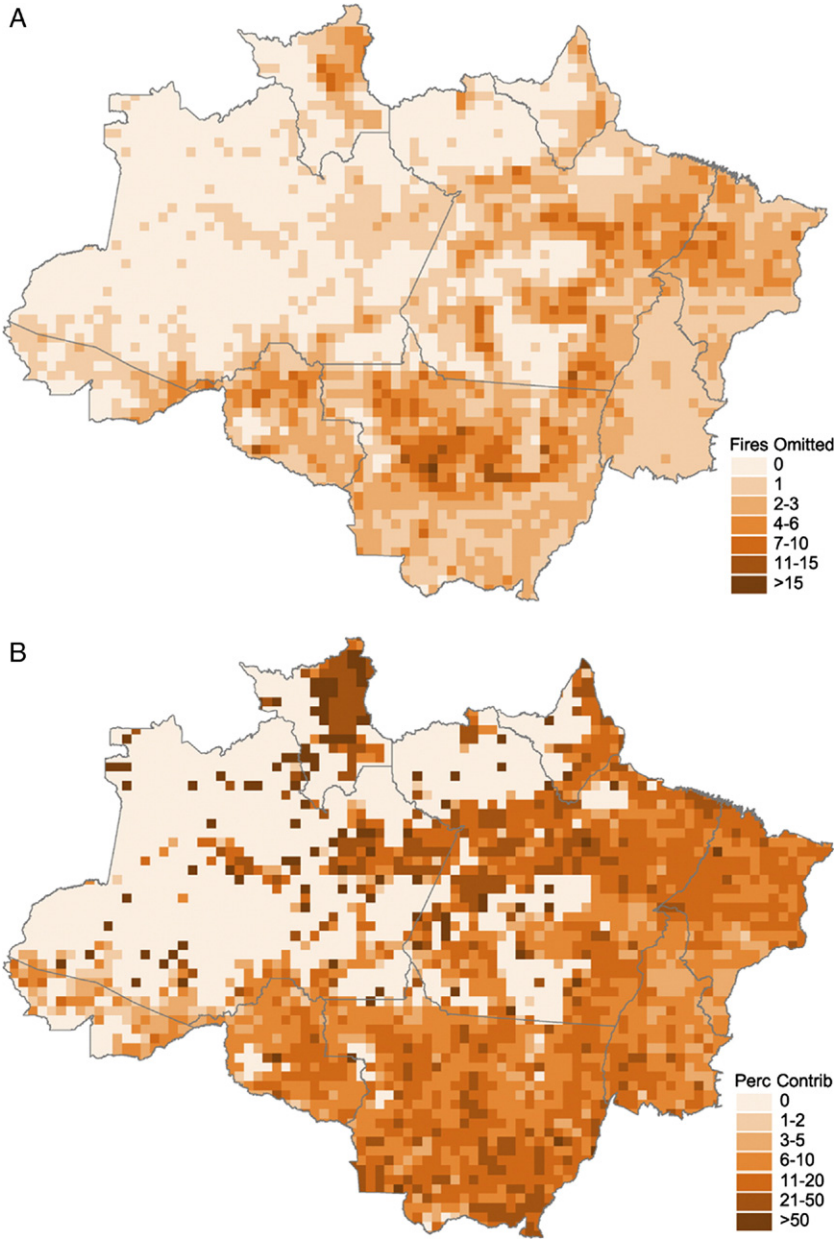

Fig. 8. Fires omitted due to clouds (A) for year 2005 and the percentage contribution (B) of cloud adjusted fires in relation to the total number of GOES WFABBA fires detected in that same year for each 40×40 km grid cell covering the Brazilian Amazon.

clouds as they do in cloudless areas (Cardoso et al., 2003; Giglio et al., 2003, 2006; Roberts et al., 2005). In order to evaluate the impact of spatial sampling, the simple approach was implemented using two different grids of 40×40 km and 120×120 km resolution each. The average fire frequency was calculated for the cloud free fraction of each grid cell based on:

$$F_{F,i} = \frac{D_{z,i}}{S_{z,i}}. \quad (10)$$

Where D_z is the number of actual fires detected within grid cell z during observation hour i, and S_z is the number of 4×4 km cloud free pixels in the same area. The number of cloud obscured pixels in each cell (i.e., 100—$S_{z,i}$ and 900—$S_{z,i}$ for the 40×40 km and 120×120 km grids, respectively) was then multiplied by Eq. (10) in order to derive the number of fires potentially missed. For both 40 km and 120 km grid resolutions used, the simple approach produced a larger number of potentially missed fires due to cloud obscuration (178,968 and 241,804 – 33% and 44% increment – respectively) as compared to the proposed methodology described above (Fig. 9). The difference was particularly important in areas where fires were unequally distributed in space, causing fire free pixels (e.g., pixels located in forested areas and distant from human activities) to be erroneously classified as fire omission areas by the simple rule approach. The use of LUTs describing the fire activity in space helped reduce this effect with the

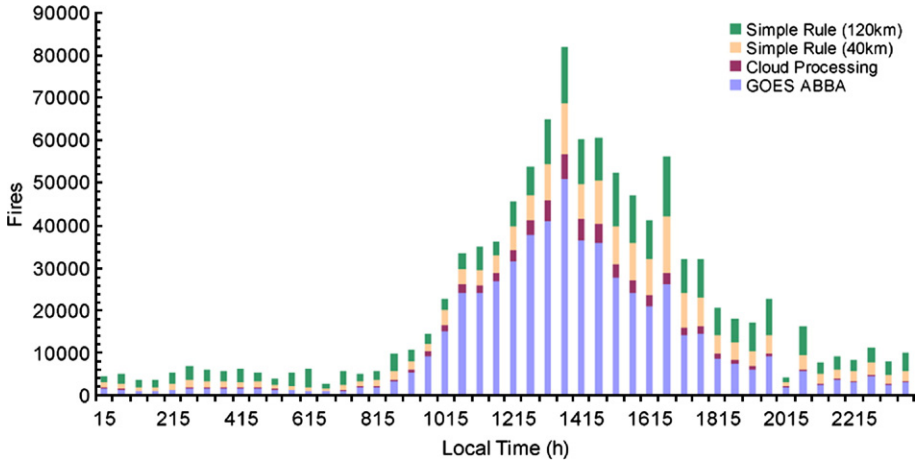

Fig. 9. GOES WFABBA fire diurnal cycle distribution for the Brazilian Amazon and the corresponding adjustment produced using the cloud obscuration processing methodology and the simple rule approach using 40 km and 120 km sampling areas.

methodology proposed by only selecting fire prone pixels during the cloud obscuration processing.

The majority of the fire omissions identified by the proposed methodology were associated with the conditions described by scenario 1, where all three observation hours $T-30$ min, T, and $T+30$ min are obscured by clouds. Average cloud coverage in the region varied between a minimum of 22% and a maximum of 78% depending on the observation hour, with the lowest values found in the areas surrounding the evergreen tropical forests in the southern and eastern parts of the basin (Fig. 10). These areas are generally composed of Cerrado (savanna) vegetation and transition forests. The highest values occurred in the western part of the basin where the hydrological cycle is enhanced by the prevalence of closed canopy forests resulting in high evapotranspiration rates and by westerly winds that bring supplemental moisture from the eastern parts of the basin. From the remote sensing perspective, this spatial distribution of fires and cloud coverage is beneficial as it minimizes the cloud obscuration problem in areas where fire activity is most pronounced (e.g., the states of Mato Grosso, Tocantins, Maranhão, and eastern Pará). Minimum cloud coverage was found to coincide with the early afternoon observation hours (Fig. 10), which has major implications for fire detection as it approaches the hour of maximum fire activity in the region (Giglio, 2007; Kaufman et al., 1998b; Prins et al., 1998). This latter finding corroborates the discussion presented in Schroeder et al. (2005) where inter-comparison analyses using multi-sensor fire data and visual confirmation of smoke plumes demonstrated the strong diurnal signature of fire activity in the region.

In order to evaluate the implications of the method implemented above we used high resolution (20 m) China–Brazil Earth Resources Satellite (CBERS-2) burn scar maps to delineate areas of fire activity relating those areas to the fire omission pixels produced. The burn scar maps were generated for the state of Acre in the western Brazilian Amazon covering the 2005 fire season in the region (July–September). Using supervised classification we produced a burnt area mosaic based on 9 CBERS images corresponding to two individual scene locations (i.e., path 180 rows 111 and 112) covering from early to late (i.e., July to October respectively) fire season in 2005. Detailed mapping of burn scars resulting from maintenance (e.g., pasture and agricultural) and conversion (e.g., slash and burn) fires was produced for an area of roughly 22,000 km^2. The quality of the burnt area mosaic was assessed using GPS points and digital photos collected from 40 h of over-flights from which all burnt area sites inspected could be visually confirmed (Foster Brown — personal communication 2005). Cloud obscuration in the region is known to significantly influence active fire products, usually limiting detection capacity irrespective of the sensor used (Brown et al., 2006). The GOES WFABBA fire counts (excluding fire category 5) were spatially aggregated into nominal 4×4 km cells along with the burn scar areas and the fire increments produced independently by the method proposed above and the simple rule approach (using 40 km and 120 km grid resolutions) and error matrices were derived (Table 2a–d). The original WFABBA active fires detected during the same period covered by the burn scar map showed an omission error of 58.3% and a commission error of 6.4%; multiple detections were frequently observed for individual 4×4 km cells across the area. Despite the reasonably high omission error, 4110 of a total of 4133 fire detections observed during the period analyzed had a spatially coincident burn scar (i.e., within ±2 km of WFABBA's fire pixel coordinate); whereas 15 of 23 fire coordinates associated with false detection had large burn scars located in the immediate vicinity of the pixel. Nevertheless, the fire pixels detected accounted for 76% of the total area burned measured for the selected plot; with the remaining 24% associated with omission showing significantly different characteristics of mean burnt area size (4 times smaller than the confirmed detections) therefore potentially falling outside the detection envelope of the GOES imager. The application of the cloud obscuration processing method showed a reduction in the omission error to 43.7% along with a minor increment of the commission error (8.8%). The pixels selected in this latter case accounted for 88% of the total area burned measured. The mean burned area size resembled the mean area size associated with the original

WFABBA fire product to within 15%. The application of the simple rule approach showed a major reduction of the omission errors for both 40 km and 120 km grids used (10% and 0%, respectively) at the cost of substantial commission errors being produced (63% and 100%, respectively). The mean burned area size described by the simple rule approach was considerably smaller (45%) as compared to the value observed with the original WFABBA data, with the burned area frequency histogram having shifted towards smaller burn scars. Despite the improvements observed primarily in terms of the reduction of omission errors, the additional fires created during processing of the cloud obscuration did not have a significant impact on the relationship between the accumulated fire counts obtained for an individual pixel area and the associated size of the burn scar measured for that same plot. That relationship remained unresolved for all four data sets analyzed (i.e., the original GOES WFABBA active fire data, the cloud adjusted numbers derived with the above methodology, and with the simple approach at 40 and 120 km), with weak correlation being observed in all cases.

5. Final remarks

Fire detection omission due to cloud obscuration is a major problem affecting remote sensing of active fires. Here we described an approach designed to address the cloud obscuration problem using high frequency geostationary observations. The methodology takes advantage of three different input data, namely precipitation estimates, a cloud mask and active fire data that are derived from the same instrument. This consideration

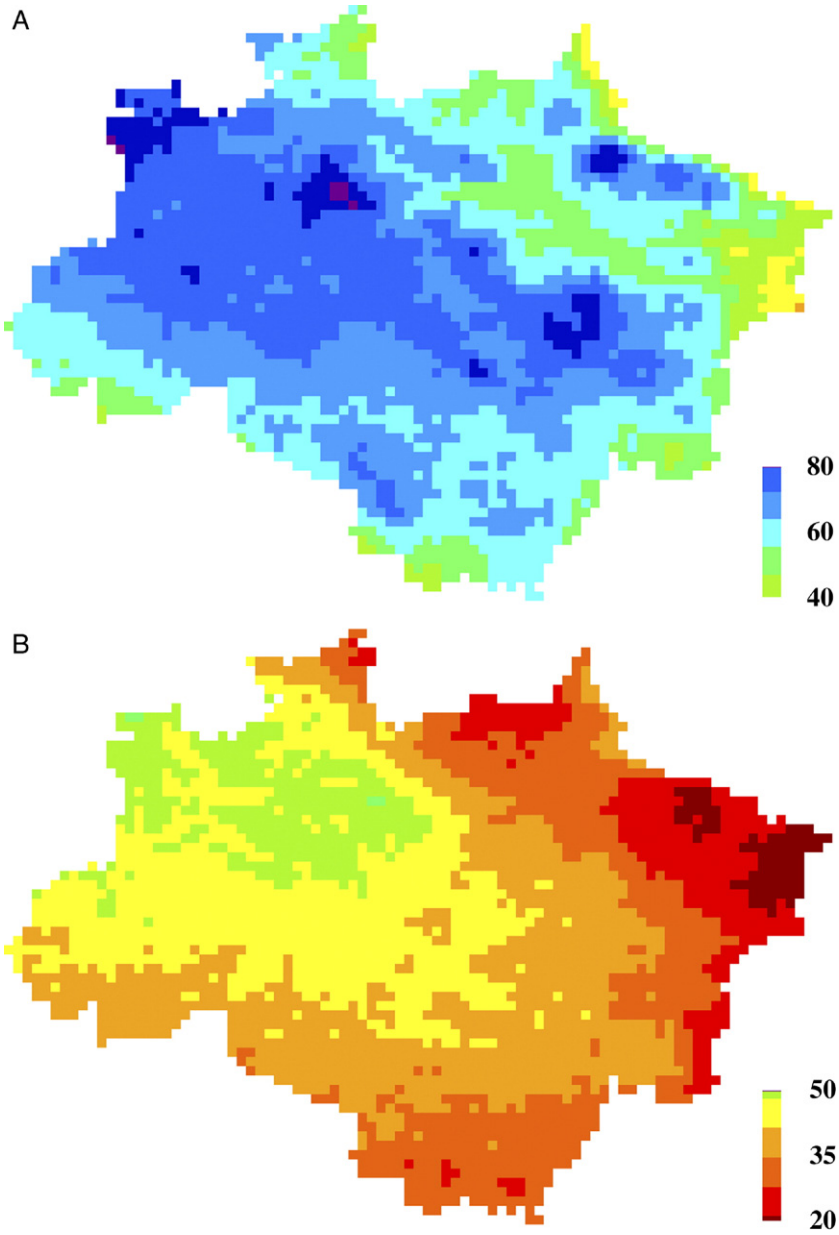

Fig. 10. Average maximum and minimum percentage cloud coverage (A and B respectively) and hours of maximum and minimum occurrence arranged in 3 hour bins (C and d respectively).

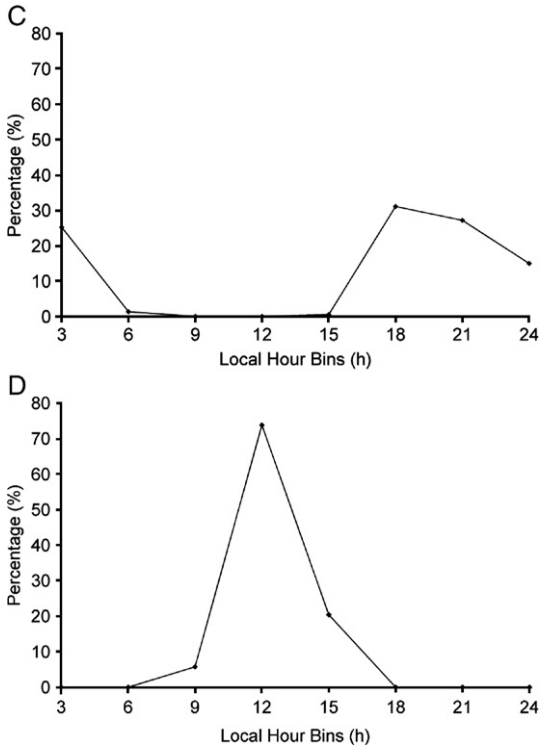

Fig. 10 (*continued*).

was especially important for facilitating data registration and also to reduce image navigation problems that can occasionally affect the GOES data. The use of recent historical active fire data along with precipitation data provided means to establish the general patterns of fire use in both space and time across the entire study area, at the same time preserving specific regional and local characteristics with the implementation of pixel based processing.

The strong correlation between the predicted fires missed and the actual fires observed demonstrated the effectiveness of the approach. In terms of the overall trends caused by cloud obscuration across the Brazilian Amazon, we observed that the net effect of fire omission was partially minimized in areas of intense fire activity as these generally coincided with the areas of minimum cloud coverage. Nonetheless, in relation to the percentage contribution of fires missed due to clouds, we found areas where fire omission was significant (Fig. 8) despite those being depicted as relatively low fire activity areas by the original WFABBA product (Fig. 1). This could signal the need to more detailed analysis of fire dynamics in areas considered to be of low priority under current regional fire management programs (e.g., northeastern Roraima).

Another important aspect presented was the partial overlap between the hours of minimum cloud coverage and of maximum fire activity as a result of a strong basin-wide fire diurnal cycle signature. The cloud adjusted numbers maintained the same fire diurnal cycle signal confirming our field observations that indicated systematic use of fires in the mid-afternoon hours as part of regional land management techniques. As compared to a more simplistic approach, the methodology was proven successful in reducing the omission errors while maintaining the commission errors nearly unchanged, and preserving the general quality of the fires described by the original fire product from WFABBA.

By means of routine updating of the LUTs used during processing, this cloud obscuration modeling technique should be capable of consistently mapping fire omission in tropical areas such as the Brazilian Amazon. While the number of fire pixels missed due to clouds could be successfully defined, additional work is required to better describe the relationship between active fires and the total area burnt which modeling of biomass emissions so much depend on.

We consider this methodology to be applicable to other geostationary systems covering different regions of the globe provided that similar data layers are available for use. The proposed cloud correction scheme can be included in the current effort by the Global Observation of Forest and Land Cover Dynamics (GOFC-GOLD) Fire Mapping and Monitoring Theme (URL:http://gofc-fire.umd.edu) to establish a global fire monitoring network from geostationary satellites. This activity, also being coordinated using principles of the Committee on Earth Observation Satellites (CEOS; URL: http://www.ceos.org) constellation concept and incorporated into the Coordination Group for Meteorological Satellites (CGMS; URL: http://www.wmo.ch/web/sat/CGMShome.html) is also a contributor to Group on Earth Observations (GEO; URL: http://www.earthobservations.org/index.html) efforts. However, we must warn for the fact that sensor dependencies (e.g., detection omission and commission rates) need to be resolved before any global analysis of the effects of clouds on remote sensing fire products is attempted.

In principle, an improved scheme to correct for cloud obscuration effects is also needed for active fire detections from polar orbiting satellites. Consistent correction is needed to

Table 2
Error matrices for evaluating the performance of the original GOES WFABBA active fire data (a), the cloud processed data (b), and the simple rule approach using 40 km and 120 km area sampling (c, d respectively) based on 20 m resolution CBERS data (our "ground truth") covering part of Acre state in western Brazilian Amazon region

	CBERS — fire	CBERS — non fire
(a)		
GOES — fire	519	8
GOES — non fire	727	117
Errors (omission/commission)	58.3%	6.4%
(b)		
Cloud processed — fire	702	11
Cloud processed — non fire	544	114
Errors (omission/commission)	43.7%	8.8%
(c)		
Simple rule (40 km) — fire	1116	79
Simple rule (40 km) — non fire	130	46
Errors (omission/commission)	10.4%	63.2%
(d)		
Simple rule (120 km) — fire	1246	125
Simple rule (120 km) — non fire	0	0
Errors (omission/commission)	0%	100%

integrate all geostationary and polar orbiting data into a long-term active fire data record as part of the Fire Disturbance Essential Climate Variable (ECV) as defined in the Global Climate Observing System (GCOS; URL: http://www.wmo.ch/web/gcos/gcoshome.html) Implementation plan. However, due to their limited observation frequency, polar orbiting satellites would require a different approach from the one presented here for the estimation of fire omission due to clouds. For instance, scenario 2 described in Section 3.3 which uses the information from adjacent observations of GOES (30 min before and after observation time *t*) would not be applicable to a polar orbiting system. Other issues such as variable imaging geometry would also impact the cloud analysis using sensors such as MODIS and AVHRR. We believe any analyses using these sensors should be treated separately.

Acknowledgments

Implementation of this study was only possible thanks to the contribution of individuals and institutions that made access to different data sets easy, namely: Gilberto Vicente (NOAA), Elaine Prins and Chris Schmidt (University of Wisconsin — Madison), Carlos Frederico Angelis and Juan Ceballos (CPTEC/INPE) as well as the data support personnel from NASA Goddard DAAC. Surface precipitation observations used for assessing the overall consistency of the GOES-based precipitation estimates were provided by the Environmental Satellite Division (DSA) of CPTEC/INPE for which we are thankful. This work is part of a doctoral dissertation project awarded a NASA Earth System Science Fellowship.

References

Alvalá, R. C. S., Gielow, R., da Rocha, H. R., Freitas, H. C., Lopes, J. M., Manzi, A. O., et al. (2002). Intradiurnal and seasonal variability of soil temperature, heat flux, soil moisture content, and thermal properties under forest and pasture in Rondônia. *Journal of Geophysical Research*, *107*. doi:10.1029/2001JD000599

Arkin, P. A. (1979). The relationship between the fractional coverage of high cloud and rainfall accumulations during GATE over the B-array. *Monthly Weather Review*, *107*, 1382–1387.

Barbosa, P. M., Stroppiana, D., Grégoire, J. -M., & Cardoso Pereira, J. M. (1999). An assessment of vegetation fire in Africa (1981–1991): Burned areas, burned biomass and atmospheric emissions. *Global Biogeochemical Cycles*, *13*, 933–950.

Bellerby, T., Todd, M., Kniveton, D., & Kidd, C. (2001). Rainfall estimation from a combination of TRMM precipitation radar and GOES multispectral satellite imagery through the use of an artificial neural network. *Journal of Applied Meteorology*, *39*, 2115–2128.

Betts, A. K., Fuentes, J. D., Garstang, M., & Ball, J. H. (2002). Surface diurnal cycle and boundary layer structure over Rondônia during the rainy season. *Journal of Geophysical Research*, *107*. doi:10.1029/2001JD000356

Boi, P., Marrocu, M., & Giachetti, A. (2004). Rainfall estimation from infrared data using an improved version of the Auto-Estimator Technique. *International Journal of Remote Sensing*, *10*, 4657–4673.

Boles, S. H., & Verbyla, D. L. (2000). Comparison of three AVHRR-based fire detection algorithms for interior Alaska. *Remote Sensing of Environment*, *72*, 1–16.

Brown, I. F., Schroeder, W., Setzer, A., Maldonado, M. L. R., Pantoja, N., Duarte, A., et al. (2006). Monitoring fires in Southwestern Amazonia rain forests. *Eos, Transactions of the American Geophysical Union*, *87*(26), 253.

Bruno, R. D., Rocha, H. R., de Freitas, H. C., Goulden, M. L., & Miller, S. (2006). Soil moisture dynamics in an eastern Amazonian tropical forest. *Hydrological Processes*, *20*, 2477–2489.

Bucini, G., & Lambin, E. (2002). Fire impacts on vegetation in Central Africa: A remote-sensing-based statistical analysis. *Applied Geography*, *22*, 27–48.

Cardoso, M. F., Hurtt, G. C., Moore, B., III, Nobre, C. A., & Bain, H. (2005). Field work and statistical analyses for enhanced interpretation of satellite data. *Remote Sensing of Environment*, *96*, 212–227.

Cardoso, M. F., Hurtt, G. C., Moore, B., III, Nobre, C. A., & Prins, E. M. (2003). Projecting future fire activity in Amazonia. *Global Change Biology*, *9*, 656–669.

Carmona-Moreno, C., Belward, A., Malingreau, J. -P., Hartley, A., Garcia-Alegre, M., Antonovskiy, M., et al. (2005). Characterizing interannual variations in global fire calendar using data from Earth observing satellites. *Global Change Biology*, *11*, 1537–1555.

Cochrane, M., Alencar, A., Schulze, M. D., Souza, C. M., Jr., Nepstad, D. C., Lefebvre, et al. (1999). Positive feedbacks in the fire dynamic of closed canopy tropical forests. *Science*, *284*, 1832–1835.

Cochrane, M., & Schulze, M. D. (1999). Fire as a recurrent event in tropical forests of the eastern Amazon: Effects on forest structure, biomass and species composition. *Biotropica*, *31*, 2–16.

Costa, M. H., & Foley, J. A. (1998). A comparison of precipitation datasets for the Amazon basin. *Geophysical Research Letters*, *25*, 155–158.

CPC — Climate Prediction Center — National Center for Environmental Prediction (NCEP) — National Weather Service (NWS), 2005, Global-merged Infra-red Brightness Temperature data set. URL:http://disc.sci.gsfc.nasa.gov/data/datapool/TRMM/01_Data_Products/06_Ancillary/01_Global_MERG_IR/index.html

CPTEC/INPE – Weather Forecast and Climate Studies Center – National Institute for Space Research – Brazil, 2005, GOES active fire detection product data set. URL: http://www.cptec.inpe.br/queimadas/queima_goes_v3.0/index_goes.html

da Rocha, H. R., Goulden, M. L., Miller, S. D., Menton, M. C., Pinto, L. D. V. O., de Freitas, H. C., et al. (2004). Seasonality of water and heat fluxes over a tropical forest in eastern Amazonia. *Ecological Applications*, *14*(4), S22–S32.

Di Bella, C. M., Jobbágy, E. G., Paruelo, J. M., & Pinnock, S. (2006). Continental fire density patterns in South America. *Global Ecology and Biogeography*, *15*, 192–199.

Dwyer, E., Pinnock, S., Gregoire, J. -M., & Pereira, J. M. C. (2000). Global spatial and temporal distribution of vegetation fire as determined from satellite observations. *International Journal of Remote Sensing*, *21*, 1289–1302.

Ebert, E. E., Janowiak, J. E., & Kidd, C. (2007). Comparison of near-real-time precipitation estimates from satellite observations and numerical models. *Bulletin of the American Meteorological Society*, *88*. doi:10.1175/BAMS-88-1-47

Elvidge, C. D., Kroehl, H. W., Kihn, E. A., Baugh, K. E., Davis, E. R., & Hao, W. M. (1996). Algorithm for the retrieval of fire pixels from DMSP Operational Linescan System Data. In J. S. Levine (Ed.), *Remote Sensing, Modeling and Inventory Development, and Biomass Burning in AfricaBiomass Burning and Global Change*, *Vol. 1* (pp. 73–85): MIT Press.

Eva, H., & Lambin, E. F. (1998). Remote sensing of biomass burning in tropical regions: Sampling issues and multisensor approach. *Remote Sensing of Environment*, *64*, 292–315.

Freitas, S. R., Longo, K. M., Silva Dias, M. A. F., Silva Dias, P. L., Chatfield, R., Prince, E., et al. (2005). Monitoring the transport of biomass burning emissions in South America. *Environmental Fluid Mechanics*, *5*, 135–167.

Giglio, L. (2007). Characterization of the tropical diurnal fire cycle using VIRS and MODIS observations. *Remote Sensing of Environment*. doi:10.1016/j.rse.2006.11.018

Giglio, L., Csiszar, I., & Justice, C. (2006). Global distribution and seasonality of active fires as observed with the Terra and Aqua Moderate Resolution Imaging Spectroradiometer (MODIS) sensors. *Journal of Geophysical Research*, *111*, G02016. doi:10.1029/2005JG000142

Giglio, L., Kendall, J. D., & Justice, C. O. (1999). Evaluation of global fire detection algorithms using simulated AVHRR infrared data. *International Journal of Remote Sensing*, *20*, 1947–1985.

Giglio, L., Kendall, J. D., & Mack, R. (2003). A multi-year active fire dataset for the tropics derived from the TRMM VIRS. *International Journal of Remote Sensing*, *24*, 4505–4525.

Giglio, L., Kendall, J. D., & Tucker, C. J. (2000). Remote sensing of fires with the TRMM VIRS. *International Journal of Remote Sensing*, *21*, 203–207.

Justice, C., Giglio, L., Korontzi, S., Owens, J., Morisette, J. T., Roy, D., et al. (2002). The MODIS fire products. *Remote Sensing of Environment*, *83*, 244−262.

Kasischke, E. S., Hewson, J. H., Stocks, B., Van der Werf, G., & Randerson, J. (2003). The use of ATSR active fire counts for estimating relative patterns of biomass burning — A study from the boreal forest region. *Geophysical Research Letters*, *30*(18), 1969. doi:10.1029/2003GL017859

Kasischke, E. S., Williams, D., & Barry, D. (2002). Analysis of the patterns of large fires in the boreal forest region of Alaska. *International Journal of Wildland Fire*, *11*, 131−144.

Kaufman, Y. J., Hobbs, P. V., Kirchhoff, V. W., Artaxo, P., Remer, L. A., Holben, B. N., et al. (1998). Smoke, Clouds, and Radiation-Brazil (SCAR-B) experiment. *Journal of Geophysical Research*, *103*, 31,783−31,808.

Kaufman, Y. J., Justice, C., Flynn, L., Kendall, J., Prince, E. M., Ward, D. E., et al. (1998). Potential global fire monitoring from EOS-MODIS. *Journal of Geophysical Research*, *103*, 32215−32238.

Kaufman, Y. J., Tucker, C. J., & Fung, I. (1990). Remote sensing of biomass burning in the tropics. *Journal of Geophysical Research*, *95*, 9927−9939.

Korontzi, S., Roy, D. P., Justice, C. O., & Ward, D. E. (2004). Modeling and sensitivity analysis of fire emissions in southern Africa during SAFARI 2000. *Remote Sensing of Environment*, *92*, 376−396.

Kummerow, C., Barnes, W., Kozu, T., Shiue, J., & Simpson, J. (1998). The Tropical Rainfall Measuring Mission (TRMM) sensor package. *Journal of Atmospheric and Oceanic Technology*, *15*, 809−817.

Menzel, W. P., Cutrim, E. C., & Prins, E. M. (1991). Geostationary satellite estimation of biomass burning in Amazonia during BASE-A. In J. S. Levine (Ed.), *Global Biomass Burning: Atmospheric, Climatic, and Biospheric Implications* (pp. 41−46): MIT Press.

Morisette, J. T., Giglio, L., Csiszar, I., Setzer, A., Schroeder, W., Morton, W., et al. (2005). Validation of MODIS active fire detection products derived from two algorithms. *Earth Interactions*, *9*, 1−25 (paper no. 9).

Nepstad, D., Moutinho, P., Dias-Filho, M. B., Davidson, E., Cardinot, G., Markewitz, D., et al. (2002). The effects of partial throughfall exclusion on canopy processes, aboveground production, and biogeochemistry of an Amazon forest. *Journal of Geophysical Research*, *107*. doi:10.1029/2001JD000360

Nepstad, D. C., Veríssimo, A., Alencar, A., Nobre, C., Lema, E., Lefebvre, P., et al. (1999). Large-scale impoverishment of Amazonian forests by logging and fire. *Nature*, *398*, 505−508.

Prins, E. M., Feltz, J. M., Menzel, W. P., & Ward, D. E. (1998). An overview of GOES-8 diurnal fire and smoke results for SCAR-B and 1995 fire season in South America. *Journal of Geophysical Research*, *103*(D24), 31821−31835.

Prins, E. M., & Menzel, W. P. (1992). Geostationary satellite detection of biomass burning in South America. *International Journal of Remote Sensing*, *13*, 2783−2799.

Roberts, G., Wooster, M. J., Perry, G. L. W., Drake, N., Rebelo, L. -M., & Dipotso, F. (2005). Retrieval of biomass combustion rates and totals from fire radiative power observations: Application to southern Africa using geostationary SEVIRI imagery. *Journal of Geophysical Research*, *110*, D21111. doi:10.1029/2005JD006018

Rozumalski, R. A. (2000). A quantitative assessment of the NESDIS Auto-Estimator. *Weather Forecasting*, *15*, 397−415.

Rudolf, B., Hauschild, H., Rüth, W., & Schneider, U. (1996). Comparison of raingauge analyses, satellite-based precipitation estimates and forecast model results. *Advances in Space Research*, *18*, 53−62.

Scholes, R. J., Ward, D. E., & Justice, C. O. (1996). Emissions of trace gases and aerosol particles due to vegetation burning in southern hemisphere Africa. *Journal of Geophysical Research*, *101*, 23677−23682.

Schroeder, W., Morisette, J. T., Csiszar, I., Giglio, L., Morton, D., & Justice, C. O. (2005). Characterizing vegetation fire dynamics in Brazil through multisatellite data: Common trends and practical issues. *Earth Interactions*, *9*, 1−26 (paper no. 13).

Van der Werf, G. R., Randerson, J. T., Collatz, G. J., & Giglio, L. (2003). Carbon emissions from fires in tropical and subtropical ecosystems. *Global Change Biology*, *9*, 547−562.

Vicente, G. A., Davenport, J. C., & Scofield, R. A. (2002). The role of orographic and parallax corrections on real time high resolution satellite rainfall rate distribution. *International Journal of Remote Sensing*, *23*, 221−230.

Vicente, G. A., Scofield, R. A., & Menzel, W. P. (1998). The operational GOES infrared rainfall estimation technique. *Bulletin of the American Meteorological Society*, *79*, 1883−1898.

Vila, D., & Lima, A. (2004). Satellite rainfall estimation over South America: The hydroestimator technique. *14th International Conference on Clouds and Precipitation, Bologna, Italy, 8–23 July, 2004*.